Daily Microwave-Derived Surface Temperature over Canada/Alaska

A. MIALON

Laboratoire de Glaciologie et Géophysique de l'Environnement, CNRS/Université Joseph Fourier de Grenoble, Grenoble, France, and Centre d'Applications et de Recherche en Télédétection, Université de Sherbrooke, Sherbrooke, Québec, Canada

A. ROYER

Centre d'Applications et de Recherche en Télédétection, Université de Sherbrooke, Sherbrooke, Québec, Canada

M. FILY AND G. PICARD

Laboratoire de Glaciologie et Géophysique de l'Environnement, CNRS/Université Joseph Fourier de Grenoble, Grenoble, France

(Manuscript received 17 March 2006, in final form 16 August 2006)

ABSTRACT

The land surface temperature variation over northern high latitudes in response to the increase in greenhouse gases is challenging because of the lack of meteorological stations. A new method to derive the surface temperature from satellite microwave measurements that improves the frequency of measurements relative to that of infrared data is presented. The daily Special Sensor Microwave Imager 25 km × 25 km Equal-Area Scalable Earth Grid (EASE-Grid) dataset provided by the National Snow and Ice Data Center in Boulder, Colorado, is processed to derive the surface temperature using the method proposed by Fily et al. A normalization approach based on the 40-yr ECMWF reanalysis (ERA-40; 2.5°) temperature diurnal cycle fitted for each pixel is applied to overcome the time acquisition variation of measurements as well as to interpolate missing data. An adaptive mask for discriminating between ice-free pixels and snow-free pixels is also applied. The resulting database is thus a new consistent hourly series of near-surface air temperatures during the summer (without snow). The mean accuracy is on the order of 2.5–3 K when compared with the synchronous in situ air temperature and different gridded datasets over Canada and Alaska. The trend over the last 10 yr confirms observed climate evolution: an increase in summer surface temperature of $+0.09° \pm 0.04°C\ yr^{-1}$, at the 90% confidence level, for Canada between 1992 and 2002, whereas a decrease of $-0.15° \pm 0.05°C\ yr^{-1}$, at the 95% confidence level, is observed for Alaska. Spatial and temporal anomalies show regional impacts of meteorological phenomena such as the El Niño extreme warm summer episode of 1998, the decrease in temperatures in 1992 in Canada following the volcanic eruption of Mount Pinatubo in June 1991, and the strong drought in the prairies in 2001. The annual sum of positive degree-days (thawing index) has been related to the permafrost distribution. The lower values of the derived thawing index (<1400 degree-days) are related well to the presence of continuous and dense discontinuous permafrost. The observed increase in the thawing index during the 1992–2002 period represents a decrease of classified permafrost area of 7%.

1. Introduction

Northern high latitudes are expected to respond more strongly to global warming than will lower latitudes [temperature increasing from around 4° to over 7°C by 2100, depending on the scenarios (ACIA 2004)]. Smith and Burgess (1999) report that 50% of the Canadian surface characterized by the presence of permafrost (from continuous to isolated) has a mean annual surface temperature higher than −2°C. Surface temperature is a key parameter because it governs the surface radiative budget and the thickness of the permafrost active layer (Oleke et al. 2003). Its survey is essential to study the surface evolution, but the lack of meteorological stations at high latitudes is a severe limitation. For example, Overland et al. (2004) studied interannual air temperature variations of weather sta-

Corresponding author address: Arnaud Mialon, Laboratoire de Glaciologie et Géophysique de l'Environnement, CNRS/Université Joseph Fourier de Grenoble, Grenoble 38402, France. E-mail: mialon@lgge.obs.ujf-grenoble.fr

DOI: 10.1175/JAM2485.1

tions for latitudes higher than 64°N. Only 16 series were available over Canada and Alaska. That means several hundred kilometers separate each local measurement.

Remote sensing appears to be an adequate alternative to fill the gaps between stations. Thermal infrared data are usually used to derive skin temperature (Jin and Dickinson 2002; Traoré et al. 1998). However, these wavelengths are sensitive to atmospheric conditions, and the presence of clouds restricts measurement acquisitions. Clear-sky conditions are required, reducing the number of available measurements, which may introduce a bias. On the contrary, microwave radiometers allow near-all-weather measurements because they are independent of solar radiation and little influenced by the atmosphere (at least at the frequencies used here). Moreover, over northern high latitudes, one or two daily measurements are available everywhere, and, last, 27 yr of continuous data are currently available. In this part of the spectrum, measurements depend mostly on emissivity and surface temperature variations. Because of these numerous advantages, several methods have been developed to derive surface temperature either based on land cover for taking into account emissivity variations or based on linear regression methods (McFarland et al. 1990). Njoku and Li (1999) showed from simulations that multichannel brightness temperature (Tb) data can be used to estimate surface temperature at an accuracy of 2°–2.5°C. Bayesian estimation techniques have also been investigated to include a priori information on sensor noise, model uncertainties, probability distributions of the parameters being estimated, and ancillary data from ground truth or other sensors (Davis et al. 1995). An improvement of this kind of approach was later proposed by Basist et al. (1998) using semiempirical adjustment techniques. Because the physics of the radiative transfer and interaction processes among soil, vegetation, and atmosphere are nonlinear, the physically based retrieval of satellite-derived temperature from Tb needs nonlinear algorithms such as iterative methods [e.g., Weng and Grody (1998), which has an accuracy of 4.4 K when compared with air temperatures T_{air}; Njoku and Li (1999), which is based on Advanced Microwave Scanning Radiometer channels (6.6, 10.7, and 18.7 GHz) and cannot be applied to Special Sensor Microwave Imager (SSM/I) data because of the different frequencies available; Pulliainen et al. (1997), which is a physically based model that requires too many input data for long time series] or neural networks [e.g., Aires et al. (2001), which is a very promising approach but is relatively tedious and is not easy to implement and duplicate].

We have thus investigated a new, simpler approach (Fily et al. 2003). This approach is briefly reported on below. However, using satellite-derived surface temperature (referred to as T_{sat}) raises a problem related to the variable temporal sampling of the data acquisition, which depends on the latitude as well as on the spacecraft orbit. We propose a normalization method based on 40-yr European Centre for Medium-Range Weather Forecasts (ECMWF) reanalysis (ERA-40) air temperature to produce hourly series of temperatures. From these series, a consistent daily mean temperature can be derived, whatever the data acquisition time and the location. Section 2 describes the datasets. Section 3 is devoted to the method, and the validation of results by comparisons with independent databases (station air temperature and other satellite data) is presented in section 4. The satellite-derived interannual temperature variations are shown and discussed in section 5 as are the annual cumulative sum of positive degree-day variations, which can be related to permafrost distribution or active-layer depth variation (Anisimov and Nelson 1996; Oleke et al. 2003).

2. Database

Microwave passive SSM/I sensors on Defense Meteorological Satellite Program (DMSP) satellites provide terrestrial brightness temperatures since August of 1987 at several frequencies (19.35, 22.2, 37, and 85.5 GHz) at both vertical and horizontal polarizations (except for 22.2 GHz, which is available only at vertical polarization). For this study, we only use data acquired during the 1992–2002 period, corresponding to the DMSP *F11* and *F13* satellites, at 37 and 19 GHz, because those channels are also available with the previous Scanning Multichannel Microwave Radiometer (SMMR) sensor (1978–87) and on the DMSP *F8* SSM/I (1988–91). We focus on DMSP *F11* and *F13* because these two sensors are cross calibrated well (Colton and Poe 1999).

Brightness temperatures are distributed by the National Snow and Ice Data Center of Boulder, Colorado (Armstrong et al. 1994). Data are presented in an equal-area grid [Equal-Area Scalable Earth Grid (EASE-Grid)], at 25-km resolution. A complete coverage of the earth is acquired in 3 days, but at high latitudes most of the surface is observed 2 times per day: once in the morning (local solar time) and once in the afternoon (Table 1).

A diurnal-cycle model of temperature is derived from reanalysis air temperature. Air temperatures at 2 m are provided by the ECMWF at 0000, 0600, 1200, and 1800 UTC at a spatial resolution of 2.5° (Uppala et al. 2005). Full-resolution ERA-40 products (about 1.125°)

TABLE 1. Equator local crossing time; corresponding orbital nodes are given in italics.

Date of availability	Platform	Local overpass time	
		Morning	Afternoon
Dec 1991–Sep 1995	DMSP *F11*	0611 *Descending*	1811 *Ascending*
Sep 1995–present	DMSP *F13*	0542 *Descending*	1742 *Ascending*

were also used for the method validation over the July and August 1999 period.

For the validation and discussion, several other independent datasets are also used. The International Satellite Cloud Climatology Project (ISCCP; Rossow and Schiffer 1991; Rossow and Garder 1993) provides a skin temperature, derived from daily composite polar and geostationary satellite infrared measurements, at 280-km resolution, covering the entire surface of the earth. Because they are based on infrared measurements, these results are limited to clear-sky conditions (Rossow and Garder 1993). We also used the gridded climate dataset from the Climate Research Unit (CRU) with a 0.5° latitude–longitude spatial resolution and monthly temporal resolution (New et al. 2000). It includes monthly means of air temperature that are compared with the satellite-derived temperature.

Last, air temperature observations at meteorological stations are used for comparison. Canadian station records are provided by Environment Canada and are available from the Meteorological Service of Canada (Downsview, Ontario, Canada). Databases for stations in Alaska come from the Climate Research Center (Fairbanks, Alaska).

Areas of interest

Northern high latitudes (i.e., higher than 45°N) are central to this project because of the presence of permafrost. Because independent datasets are available for validation over Canada, this first effort is focused on the northern part of the North American continent. A mask is applied to exclude coastal pixels from our study. The difference between the original resolution (27 km × 18 km at 37 GHz) and the interpolated grid (25 km) leads to coastal pixels contaminated by close open water (lakes larger than 25 km and oceans).

Because the surface temperature determination method developed by Fily et al. (2003) is not applicable when snow is present, permanent snow-/ice-covered surfaces are excluded based on a land cover dataset (Latifovic et al. 2004). Seasonal snow-covered pixels for each image are selected using 19- and 37-GHz data as described by Mialon et al. (2005a,b).

3. Method

a. Temperature derived from satellite measurements

Fily et al. (2003) developed a simple method to compute a satellite-derived temperature (hereinafter T_{sat}) from microwave brightness temperatures. The brightness temperature at the satellite level is given by

$$\text{Tb}_p = \varepsilon_p T_{\text{sat}} \tau + (1 - \varepsilon_p) T_{\text{atmos},\downarrow} \tau + T_{\text{atmos},\uparrow}, \quad (1)$$

where p is polarization [vertical (V) or horizontal (H)], Tb is brightness temperature, ε_p is surface emissivity, T_{sat} is satellite-derived temperature, τ is atmospheric transmission, $T_{\text{atmos},\downarrow}$ is downward atmospheric brightness temperature, and $T_{\text{atmos},\uparrow}$ is upward atmospheric brightness temperature.

An empirical linear relationship (Fily et al. 2003) between emissivity at vertical and horizontal polarizations was found: $\varepsilon_V = a\varepsilon_H + b$, where $\varepsilon_{V/H}$ stands for surface emissivity at vertical and horizontal polarization, respectively, and a and b are the linear regression coefficients from Fily et al. (2003): $a = 0.5022$ and $b = 0.4838$ at 37 GHz. From the two above equations the satellite-derived temperature can be computed:

$$T_{\text{sat}} = [\text{Tb}_V - a\text{Tb}_H - (1 - b - a)\tau T_{\text{atmos},\downarrow} - (1 - a) T_{\text{atmos},\uparrow}]/(\tau b). \quad (2)$$

Only the 37-GHz T_{sat} are used hereinafter because the penetration depth is smaller than it is for the 19-GHz channel, making them less sensitive to soil moisture, and because the spatial resolution at this frequency is closer to the EASE-Grid resolution: 27 km × 18 km at 37 GHz as opposed to 69 km × 43 km at 19 GHz.

SENSITIVITY ANALYSIS

Fily et al.'s (2003) method is based on a simple relationship, assuming constant atmospheric contributions (atmospheric brightness temperature and transmission), computed with the atmospheric module of the Helsinki University of Technology (HUT) snow emission model (Pulliainen et al. 1999), assuming no clouds and a mean constant integrated water vapor content of 1.5 g cm^{-2}. A sensitivity analysis on a, b, and atmospheric components is done to estimate the error on the resulting T_{sat}. From the same dataset used by Fily et al. (2003), relative errors on linear regression coefficients a and b are estimated to be lower than 1%. Brightness temperatures range from 245 to 276 K, with a 0.1-K step. Atmospheric components (transmission and brightness temperature) are computed (HUT model; Pulliainen et al. 1999) for various atmospheric conditions: from 0 to 5 g cm^{-2} for clear and different cloudy

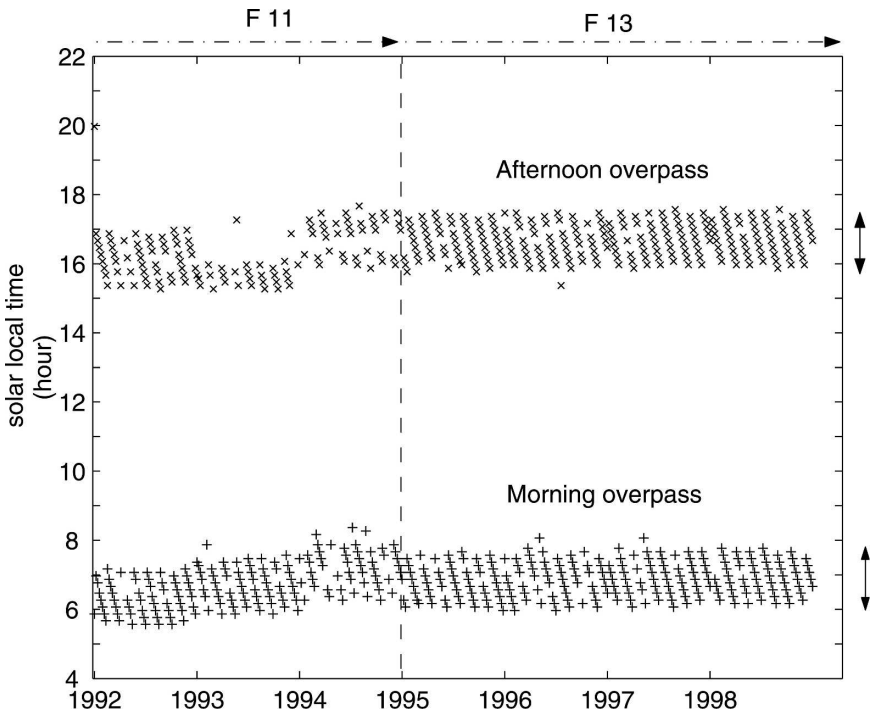

FIG. 1. Local solar time of measurement during summer days, between 1992 and 1998; the two orbital overpasses provide one measurement in the morning and one in the afternoon: DMSP *F11* satellite is used for summer 1992–summer 1994, and *F13* is used for summer 1995–present. Arrows on the right mark the day-to-day range of measurement time.

skies (fair-weather cumulus cloud, fog, heavy haze, cirrostratus, cumulus).

The errors tend to be balanced in Eq. (2), and the resulting computed T_{sat} distribution leads to a mean difference of −0.19°C (RMSE of 0.71°C), with T_{sat} derived with Fily et al.'s (2003) parameters. This confirms the Fily et al. (2003) conclusions considering the small influence of the atmosphere on the derived temperature.

b. Satellite-derived temperature daily normalization

From satellite overpasses, a maximum of only two temperatures can be derived daily: one near 0600 (equator-crossing local time) and one near 1700 (equator-crossing local time; see Table 1). From day to day, local measurement time may vary because (see Fig. 1) 1) different sensors may have a slightly different overpass time (see Table 1), 2) sensors record brightness temperatures across a 1400-km swath, which implies a 2-h difference between extreme positions in the scan (shown by arrows on Fig. 1), and 3) satellite overpass-time drifts during the lifetime of the satellite.

Measurement time is given in Fig. 1 for the pixel corresponding to Baker Lake station (64°18′N, 96°4′W; Nunavut, Canada). Measurement time in the morning occurs between 0600 and 0800 (local solar time), and overpass time in the afternoon occurs between 1530 and 1800 (local solar time). Moreover, the 1400-km swath and the satellite orbit entail that data are not available every day.

It is then difficult to compare satellite-derived temperatures obtained by different sensors or even to compare with other climatic sources based on mean daily temperatures. For consistent time series, it is consequently necessary to interpolate accurately the gaps between measurements by taking into account the diurnal cycle.

In the best case, two data per day are available, which is not enough to obtain a diurnal cycle with an interpolation function (a sinusoidal function was tested without satisfactory results): other information is needed. Fily et al. (2003) showed a good correlation between T_{sat} and air temperature reported at meteorological stations. ERA-40 air temperatures are given every 6 h at a spatial resolution of 2.5°C. An hourly diurnal cycle is obtained from ERA-40 data interpolated with a spline cubic function. This interpolation technique has the advantage of producing smooth series at measurement points. Aires et al. (2004) showed the ability to obtain an hourly diurnal cycle from cubic-

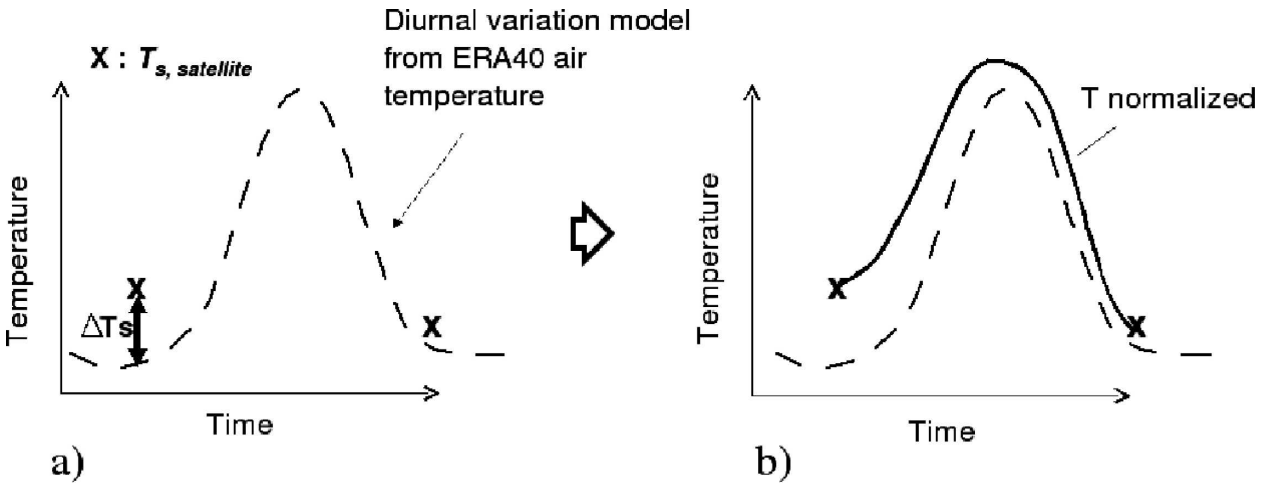

FIG. 2. Normalization process: applying ERA-40 diurnal cycle (dashed line) to satellite-derived temperature (X) derived from SSM/I sensor leads to normalized (hourly) series (continuous).

spline interpolation of 3-hourly ISCCP surface skin temperatures. The principles of this approach are presented in Fig. 2. One or two ΔT (i.e., T_{sat} minus ERA-40 temperature interpolated at a given hour) are available every day. A linear interpolation is then used to obtain hourly ΔT series. Adding hourly ΔT series to hourly ERA-40 temperature series results in an hourly temperature series (hereinafter referred to as normalized temperature $T_{sat,norm}$) fitted with satellite-derived temperatures from Eq. (2). Figure 3 presents an example for the pixel corresponding to the Baker Lake weather station during the second week of July in 1999 (yeardays 188–196). The normalized temperature series (continuous line on Fig. 3) are in good agreement with observed air temperatures recorded at the station (black dots in Fig. 3).

The spline interpolation was also tested for different combinations of 6-h measurement points to check the effect of UTC ERA-40 reference time relative to variable local time across Canada and Alaska. A maximum bias of 0.4°C is found as a result of the interpolation technique being based on varying sampling-time point.

We also show that the mean T_{sat} data, that is, not normalized for correcting the time acquisition variation and missing data, exhibit larger differences with in situ measurements (Mialon 2005). For example, at Baker

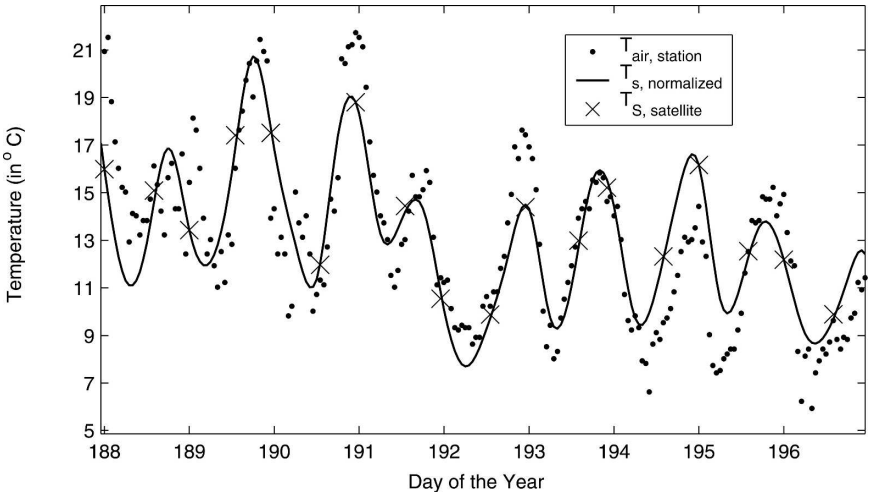

FIG. 3. Example of the satellite-derived normalized temperature series (black line) for pixels relative to Baker Lake (64°18′N, 96°4′W) meteorological station. Air temperature observations (filled circles) and the raw temperature derived from SSM/I data (times signs) are presented.

TABLE 2. Mean summer temperature differences and RMSE between normalized temperatures from SSM/I data and in situ air temperatures.

	Land cover category from 1 Jul to 31 Aug	Studied summers for $T_{sat,norm} - T_{air,station}$	Mean difference (°C)	RMSE
Baker Lake, 64°18′N, 96°4′W	Tundra	1992–99	1.3	2.8
La Tuque, 47°24′N, 72°47′W	Closed forest	1992–99	−3.0	3.8
Churchill, 58°43′N, 94°07′W	Shrubland	1999	2.7	3.4
Old Aspen, 53°63′N, 106°20′W	Closed forest	1999	−1.1	2.5
Kugluktuk, 67°82′N, 115°14′W	Tundra	1992–99	2.1	3.6
North Battle Ford, 52°77′N, 108°26′W	Cropland	1992–99	0.1	2.7
Medicine Hat, 50°02′N, 110°72′W	Grassland	1992–02	4.2	5.3
Kuujjuaq, 58°10′N, 68°42′W	Tundra	1992–02	1.4	2.6

Lake station air temperatures are lower than $T_{sat,norm}$ of −1.25°C (RMSE of 1.36°C), and they are lower than daily mean morning T_{sat} (AM) and evening T_{sat} (PM) of −1.70°C (RMSE of 1.76°C) during the summers of 1992–2000. At La Tuque station for the same period, air temperatures are lower than mean $T_{sat,norm}$ of −3.87°C (RMSE of 4.05°C), and they are lower than daily mean of T_{sat} AM and T_{sat} PM of −3.95°C (RMSE of 4.15°C).

4. Validation of a satellite-derived temperature

The meaning of the microwave satellite–derived temperature is difficult to characterize because it depends on the land cover (Dash et al. 2002). Because of radiation penetration, the derived temperatures are spatially variable following the surface properties, such as vegetation density and type (height). It appears that the derived parameter is linked to the land surface temperature equivalent to the skin temperature over bare soil (such as tundra) and to the near-surface air temperature over thin vegetation layers such as prairies (Prigent et al. 2003).

For forested surfaces, the satellite-derived temperature refers to an average effective radiative temperature integrated over the canopy height (Betts et al. 1996). It is thus linked to the air temperature above the ground for vegetated and forested areas. Over a wide surface as measured by SSM/I sensors, it represents a mean state weighted by all surface conditions. These spatial and physical aspects thus render the comparison between these different temperatures difficult, and this problem was carefully checked through comparisons with different datasets over different time periods.

Meteorological weather stations are always located in open areas not influenced by trees, and air temperatures are measured in sheltered box 1.5 m high. On the other hand, satellite-derived temperatures correspond to large areas (625 km^2), characterized by variable land cover heterogeneity. Moreover, meteorological phenomena, such as wind or direct solar flux, may imply differences between air-sheltered temperatures and satellite-derived temperatures. The comparison between these different temperatures (air station and surface temperature derived from satellite sensor) must thus be taken with caution.

a. Validation with meteorological station data

Meteorological-station air temperatures over Canada acquired in different land cover regions are compared with daily mean temperatures derived from $T_{sat,norm}$. Table 2 summarizes the results of this comparison. Different summers are studied (second row) depending on data availability. It appears that at Medicine Hat (50°02′N, 110°72′W), located in the Canadian prairies, T_{sat} is better related to skin temperature rather than air temperature. Influenced by solar radiation, the satellite-derived temperature of bare soils and sparsely vegetated surfaces is warmer than air temperature measured in a sheltered box. This may explain the large bias observed (4.2°C).

In the case of a dense canopy cover, different behavior is observed. To illustrate this assertion, in situ observations from the Boreal Ecosystem–Atmosphere Study (BOREAS) Old Aspen site (53°63′N, 106°20′W, Saskatchewan Prince Albert National Park), which is located within the canopy area (aspen forest and hazel), are analyzed. Measurements are provided by the Boreal Ecosystem Research and Monitoring Site (BERMS) project, which is part of BOREAS (Neumann et al. 1995). Several temperatures are provided at this site: air temperature at different heights (1, 4, 18, and 37 m above the ground) and soil temperature at various depths (−2, −5, and −10 cm). Figure 4 presents a comparison between $T_{sat,norm}$ (for the EASE-Grid pixel containing the Old Aspen site) and two temperature series: air temperature at 1-m height and soil temperature at 2-cm depth. It is clear that the information derived from our study is close to the air temperature

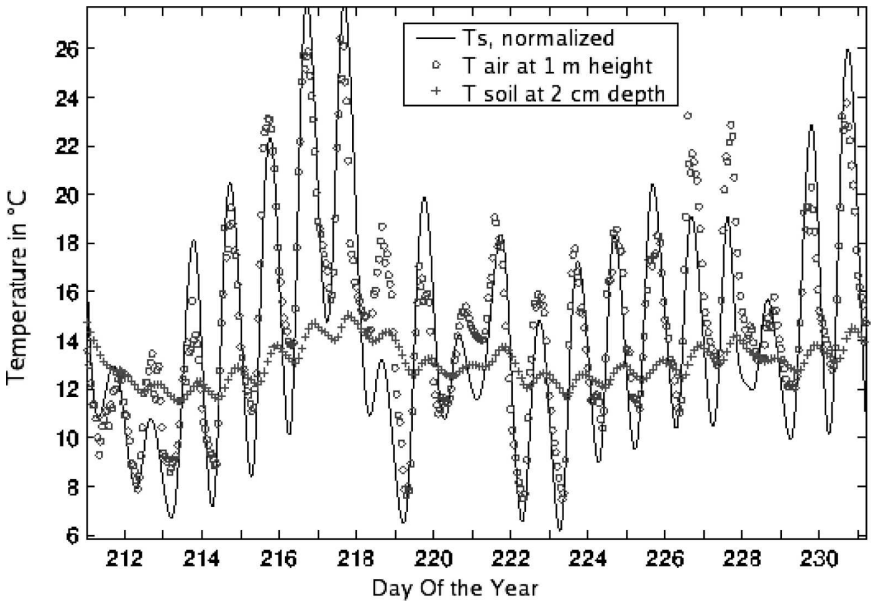

FIG. 4. Comparison between in situ observations: air temperature at 1-m height (open circles) and soil temperature at 2-cm depth (plus signs) at Old Aspen site (53.629°N, 106.2°W), Canada, and normalized temperature (continuous line). Period is between 31 Jul (yearday 182) and 18 Aug (yearday 230) 1999.

and not to soil temperature. Moreover, daily mean temperature is reproduced well with the SSM/I-derived product slightly colder than the daily mean air temperature (difference of −1.1°C and RMSE of 2.5°C; Table 2). Results also show that the temperatures at higher heights give similar errors (RMSE between 3.2° and 2.5°C from 37 to 1 m, respectively; not shown).

In conclusion, for all vegetated sites, the average difference between the mean daily satellite-derived temperatures and in situ measurements is on the order of −0.3° (RMSE = 2.9°C), and it is of +3°C (RMSE = 4°C) for the sites in the tundra and prairies.

b. Comparison with gridded temperatures

Comparisons with other types of data, such as reanalysis, gridded meteorological, and satellite infrared skin temperature were carried out over the entire study area (Canada–Alaska).

We focus on July and August of 1999 because, for these months, full-resolution (N80 quasi-regular Gaussian grid, about 1.125°) ERA-40 data were available. Hourly $T_{\text{sat,norm}}$ series were computed, and daily mean temperatures were derived. The daily mean pixel-by-pixel differences with different datasets for the summer of 1999 are shown in Fig. 5. Our satellite-derived datasets are compared with the full-resolution ERA-40 air temperatures (Fig. 5a) and skin temperature (Fig. 5b) products and with the ISCCP skin temperature data (Fig. 5c). Observed differences averaged over the whole area are reported in Table 3.

The detailed 1 km × 1 km land cover map (Fig. 5d) of the study area allows one to relate the observed differences between the datasets as a function of the main vegetation cover type. Figure 5 shows that in regions characterized by low/open vegetation, $T_{\text{sat,norm}}$ is more closely related to skin temperatures than to air temperatures. Relative to air temperatures, $T_{\text{sat,norm}}$ are warmer over tundra (northern part of Canada) and the prairies (the southwest of Canada). Over high canopy and densely vegetated surfaces, $T_{\text{sat,norm}}$ are slightly lower than the temperatures in the other datasets. The difference between surface and air temperature is largely driven by energy exchanges at the land surface boundary. With denser vegetation, the evaporation rate increases and the sensible heat flux decreases, inducing negative ($T_s - T_{\text{air}}$) difference during daytime (Betts et al. 1996). Over high elevations (the west of Canada; the Rocky Mountains), $T_{\text{sat,norm}}$ are colder than air and skin temperatures because of the ERA-40 spatial resolution (which is lower than SSM/I resolution), which may lead to an underestimation of the altitude, with the highest parts being smoothed when averaging elevation over large areas. The ISCCP skin temperature exhibits large positive differences over the northwest coast of Canada/Alaska and over eastern Canada (Fig. 5) that

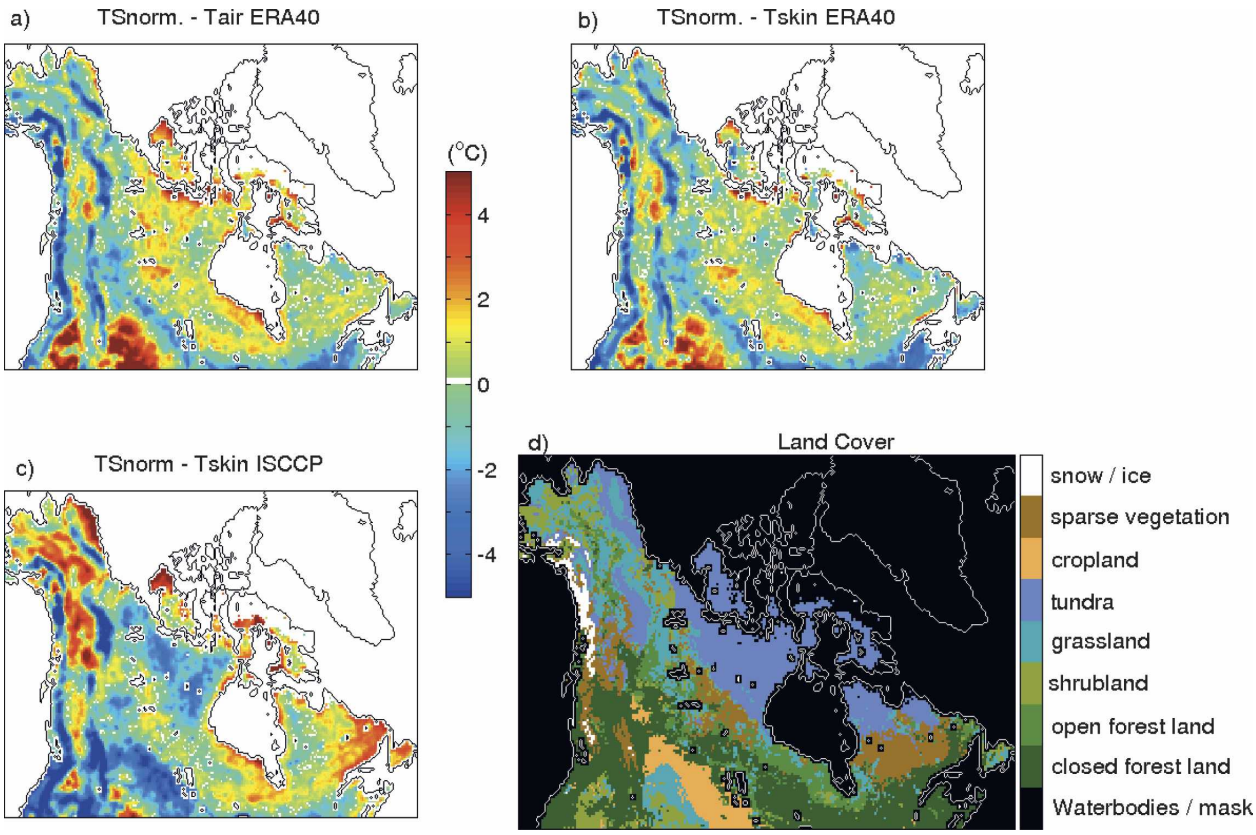

FIG. 5. Summer 1999 daily mean temperature differences between the satellite-derived $T_{sat,norm}$ and (a) ERA-40 full-resolution air temperature, (b) ERA-40 full-resolution skin temperature, and (c) ISCCP skin temperature. (d) The land cover map of the area from Latifovic et al. (2004).

may be a consequence of bias of ISCCP temperatures induced by cloud-free atmosphere selection, a necessary limitation for infrared measurements. As an example, over the southern part of the prairies, differences between $T_{sat,norm}$ and ERA-40 skin temperatures may reach 2°–3°C. For a clear-sky atmosphere, the solar flux warms the surface of the prairies, increasing the difference between surface temperature and air temperature in sheltered boxes (Prigent et al. 2003).

Table 3 summarizes the spatially averaged mean difference over Canada/Alaska. For the overall area, the observed differences remain below 1° of range, with RMSE between 1.5° and 2°C. The satellite-based dataset appears closer to the ERA-40 air temperature ($\Delta T = -0.06 \pm 1.77$°C) than to other datasets. We also compared our dataset with the CRU gridded meteorological air temperature (New et al. 2000). A mean difference of 1.2°C and RMSE of 2.6°C are found over the 1992–2002 period. Spatial differences (not shown) present the same features as are observed in Fig. 5.

In conclusion, our database compares well to in situ observations, reanalysis, and gridded meteorological datasets, with an accuracy on the order of 2°–3°C. The variations of difference between satellite-derived surface temperature and air temperature ($T_{sat} - T_{air}$) appear to be modulated by the land cover type at local scale (Table 2 and Fig. 5). Vegetation type and fractional cover affect the surface radiative transfer as well as the latent and sensible fluxes, generating, as expected, a positive difference over bare soil (the soil is warmer than the air), whereas a negative difference is observed over forested areas as confirmed by compari-

TABLE 3. Mean differences and RMSE between summer 1999 daily mean temperatures $T_{sat,norm}$ and full-resolution ERA-40 air temperatures, full-resolution ERA-40 skin temperatures, and ISCCP skin temperatures.

	Mean difference (°C)	RMSE (°C)
$T_{sat\ norm} - T_{air}$ ERA-40	−0.06	1.77
$T_{sat,norm} - T_{skin}$ ERA-40	−0.31	1.52
$T_{sat,norm} - T_{skin}$ ISCCP	−0.73	2.09
T_{skin} ERA-40 − T_{air} ERA-40	0.30	0.73
T_{skin} ERA-40 − T_{skin} ISCCP	−0.18	2.09

son with in situ observations (higher air temperature than surface temperature, mainly because of the vegetation evaporation cooling effect, among others). At the continental scale, the satellite-derived surface temperature is correlated well with the near-surface air temperature, with a monthly mean difference of less than 0.7°C (Table 3).

The major interest of the method presented here is that it generates a consistent gridded dataset of daily mean temperatures, which can compensate for the problem of the lack of stations in the northern latitudes. Indeed, because reanalyses are constrained by weather station measurements, large interpolation errors may be expected in gridded meteorological data. Moreover, the derived parameter is spatially representative of the state of the surface over an area of 25 km × 25 km, instead of local weather station measurements that are possibly not representative of the surrounding area (such as for those in coastal areas). Thus, the main advantage of the satellite data is to give a high-resolution surface temperature even where almost no in situ measurements are available. There, the good comparison with ERA-40 can be considered as a validation of the reanalysis product in those areas.

5. Results

In this section, our $T_{\mathrm{sat,norm}}$ product is used to present interannual variations, as well as to derive a climate index related to surface energy budget.

a. Interannual variation of temperature

We present here different results relevant to the 1992–2002 period. Figure 6 shows the spatial and temporal variation of summer daily means of the normalized satellite-derived temperature anomalies over Canada and Alaska. The use of satellite data provides interesting detailed spatial variations, because regions are affected by specific events. For example, during the summer of 1998, following the El Niño extreme event (season 1997/98), important impacts in Canada such as a decrease in snow cover extent (Brown and Alt 2001), earlier lake breakup (Walker 1997), and a sharp increase in temperature were reported (Atkinson et al. 2006). As observed in Fig. 6, most of Canada, except for the eastern part, underwent a strong warming anomaly. In contrast, 1992 was influenced by the Mount Pinatubo eruption (in June of 1991; Hansen et al. 1992, 1996), the cooling effect of which affected the southwest part of Canada (Fig. 6) and was still ongoing during the summer of 1993 (Lucht et al. 2002; Hansen et al. 1996).

Considering the entire study area, that is, Canada and Alaska (latitudes >45°N), Fig. 7 presents the interannual variability of the mean daily summer (for the months of July and August) temperature from this new satellite database (continuous line with dots, Fig. 7) relative to the mean daily summer (also for months of July and August) ERA-40 air temperature (dashed line with plus signs in Fig. 7). Note that some satellite data are missing over areas in western Canada during 1994, explaining the missing mean temperatures for that year. The same trend is observed for both series, with a temperature increase of $+0.08° \pm 0.04°\mathrm{C\ yr^{-1}}$ (with 90% confident with the Student's t test) for the satellite-derived database over the 1992–2002 period. Even if the satellite-derived absolute temperature is slightly warmer (+0.44°C with RMSE of 0.45°C) than the ERA-40 air temperatures, the trend is similar to the one computed from the ERA-40 database ($+0.09 \pm 0.03°\mathrm{C\ yr^{-1}}$). This is confirmed by the comparison shown in Fig. 8 for the anomaly trends derived from meteorological stations.

Climate report (ACIA 2004) analyses are mostly based on weather-station air temperature interannual variability. The relative trends for $T_{\mathrm{sat,norm}}$ and air temperature are in good agreement either for Canada (Fig. 8, top) or for Alaska (Fig. 8, bottom). Two particularly warm years (1998 and 2001) are observed in Canada, as mentioned earlier. Environment Canada reports that the warmest four summers in the 1948–2002 period are 1998, 1989, 2001, and 1994 (in descending order). During this short time period (1992–2002), Canada is subject to an increase in temperature of $0.09° \pm 0.04°\mathrm{C\ yr^{-1}}$ (while air temperatures indicate an increase of $0.07° \pm 0.04°\mathrm{C\ yr^{-1}}$). On the other hand, Alaska sustained a decrease in temperature of $-0.15° \pm 0.05°\mathrm{C\ yr^{-1}}$ (with a statistical confidence Student's t test of 95%), also observed for air temperatures at meteorological stations ($-0.08° \pm 0.03°\mathrm{C\ yr^{-1}}$ for the same 1992–2002 period) reported by Overland et al. (2004) for the Nome, Barrow, and Fairbanks, Alaska, stations.

However, these trends are influenced by cool years at the beginning of the period and warm years at the end of the period, which is, moreover, climatologically short. These trends are not representative of temperature evolution over the last century, but they validate the method used in this work.

b. Thawing degree-days

A climate index often used in glaciological and climate studies is the cumulative degree-days, defined as the cumulative sum over a year of daily mean temperatures higher than a threshold. Anisimov and Nelson

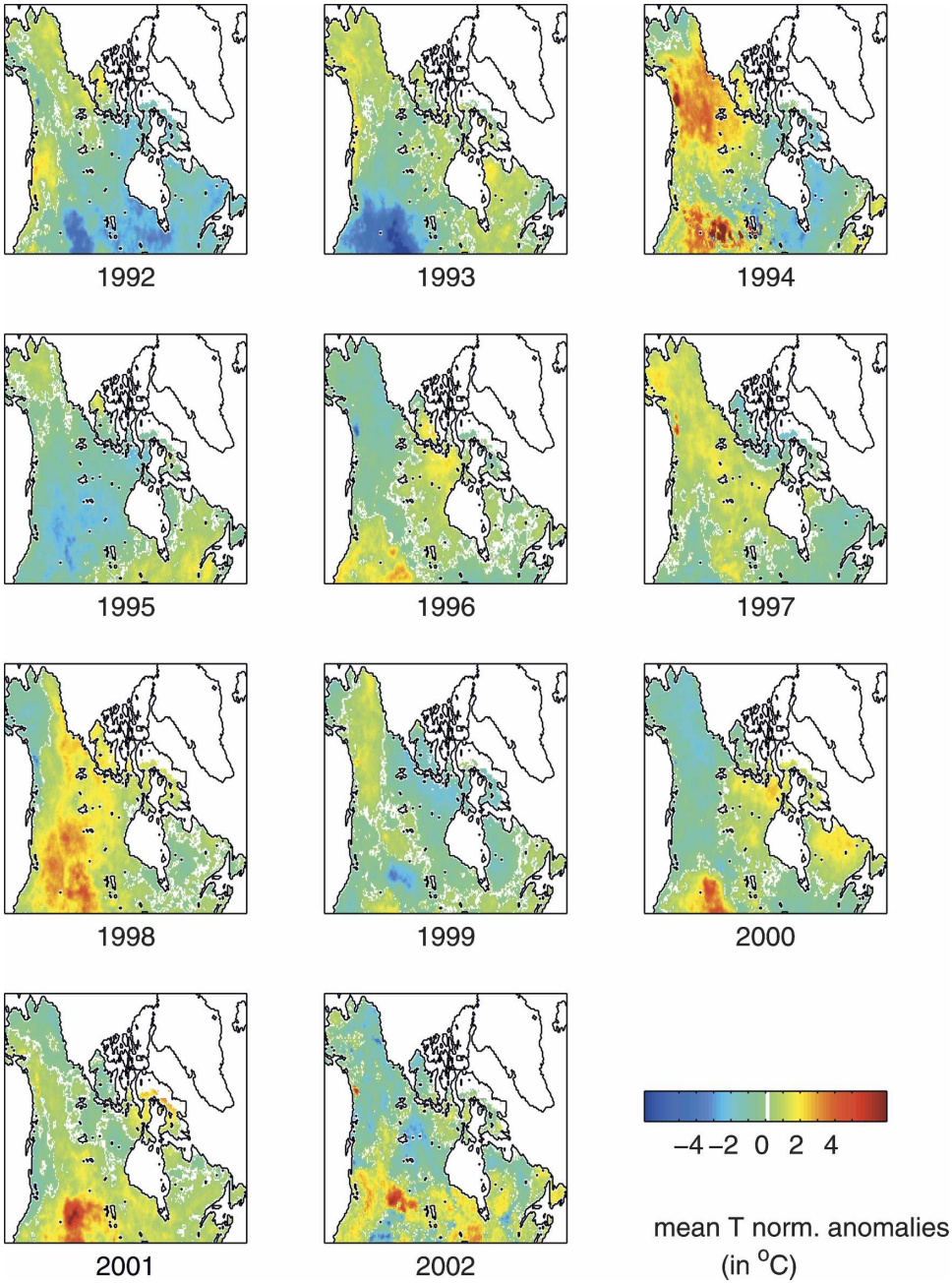

FIG. 6. Summer mean normalized satellite-derived temperature spatial anomalies over the 1992–2002 period.

(1996) used this index associated with a threshold of 0°C: the thawing index, for studying a relationship with permafrost distribution along with a freezing degree-day index (same index but for negative temperatures). Oleke et al. (2003) also found that the active layer of permafrost (the soil layer at the surface that freezes during winter and melts during summer) can be linked to the square root of the thawing degree-days following a simplified surface energy budget equation. They concluded that the maximum thaw depth of the active layer of permafrost is driven by the annual cumulative surface temperature. Smith and Burgess (1999) also linked permafrost regional distribution to the temperature climatological pattern. Soil temperature generally responds to the forcing of air temperature but in a complex way, including the vegetation, snow, soil moisture,

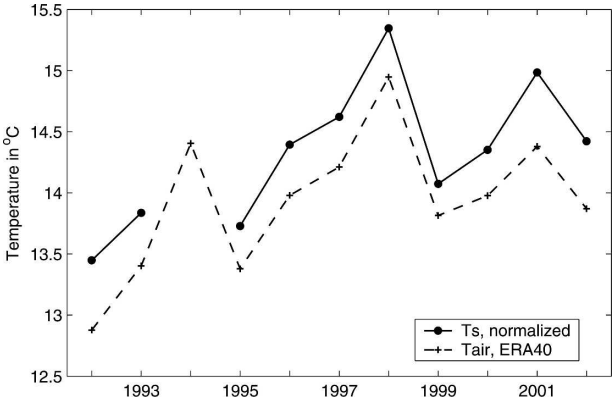

FIG. 7. Interannual variation of mean summer satellite-derived normalized temperature (solid line with filled circles) and mean ERA-40 temperature (dashed line and plus signs) for Canada and Alaska.

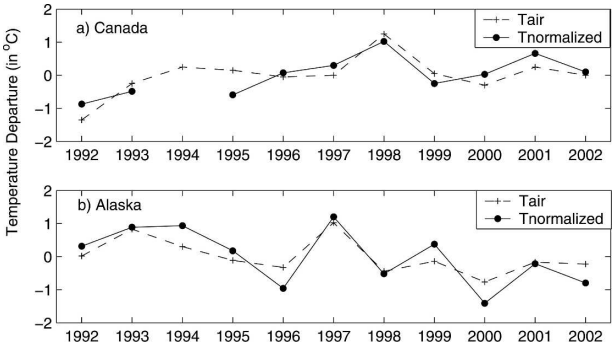

FIG. 8. Trends of the summer mean anomalies for normalized satellite-derived temperature (continuous line) and meteorological air temperature (dotted line) over the 1992–2002 period for (a) Canada and (b) Alaska.

and other climate variable effects (Zhang et al. 1999).

To derive this thawing index, we sum over a year the daily mean temperatures warmer than 0°C (positive annual degree-days) obtained during the snow-/ice-free period (Mialon et al. 2005a) on a pixel-by-pixel basis. This index is hereinafter labeled the microwave thawing index (MWTI).

Figure 9 compares the mean (1992–2002) spatial distribution of MWTI over Canada and Alaska with the permafrost distribution from Heginbottom et al. (1993) showing good agreement with the one computed by Oleke et al. (2003) from their heat conduction model, with lowest values related to higher latitudes and mountains (western Canada), whereas the highest values of the thawing index characterize the Canadian prairies.

From choosing two specific values of MWTI, derived from a comparison with the permafrost distribution, three classes are defined. Areas characterized by MWTI $>$ 2000 degree-days are related to no permafrost areas (white areas on right-hand side of Fig. 9), whereas areas characterized by MWTI $<$ 1400 degree-days seem to be related to continuous permafrost (black area on left-hand side of Fig. 9). This last class covers 3.90×10^6 km^2 as compared with the 2.30×10^6 km^2 reported for the Heginbottom et al. (1993) continuous permafrost area (black area on the left-hand side of Fig. 9). Main differences appear in western Canada, corresponding to the Rocky Mountains (mountain permafrost). When selecting lower-altitude areas (lower than 500 m), surfaces with low MWTI cover 2.51×10^6 km^2, which agrees in space and amplitude with the Heginbottom et al. (1993) continuous permafrost location (2.02×10^6 km^2).

However, it must be outlined that it is difficult to fix detailed boundaries for comparing these two maps because of the different spatial sampling and the short period of satellite observations with respect to the long characteristic time of permafrost process. Indeed, because SSM/I sensors measure a brightness temperature for a 625-km^2 area, MWTI values are relative to a mean state of this large area. Sporadic or patch permafrost may cover a different class within a pixel, and so it could be associated with our first class (blue one on the right-hand side of Fig. 9). Thus, the Heginbottom et al. (1993) category boundaries between the different types of permafrost might be different from the sensor point of view.

Taken as a spatially and temporally consistent climate index linked to the permafrost behavior, the MWTI variation can be used to analyze the impact of a warming trend (in amplitude and duration). Interannual variations of the averaged thawing index over the whole of Canada/Alaska show a global increase of 23.6 ± 6.2 degree-days yr^{-1} (statistically significant at 97.5% with Student's t test). This result is a combination of a longer thawing period (Brown 2000), that is, an increase in the number of days with a daily mean temperature above 0°C, and an increase in summer daily mean temperatures. This trend, computed over the short period of 1992–2002, appears to be stronger than the one reported by Zhang et al. (2000) for Canada: +4.4°C days yr^{-1}. Their trend applies to a longer time series (1971–2001) than was used in our work. In terms of surface evolution for the 1992–2002 period, the class characterized by small MWTI (lower than 1400 degree-days yr^{-1}) decreases from 4.07×10^6 km^2 at the beginning of the period to 3.78×10^6 km^2 at the end (−7%). This result confirms the significant impact of northern warming during the last decade (ACIA 2004).

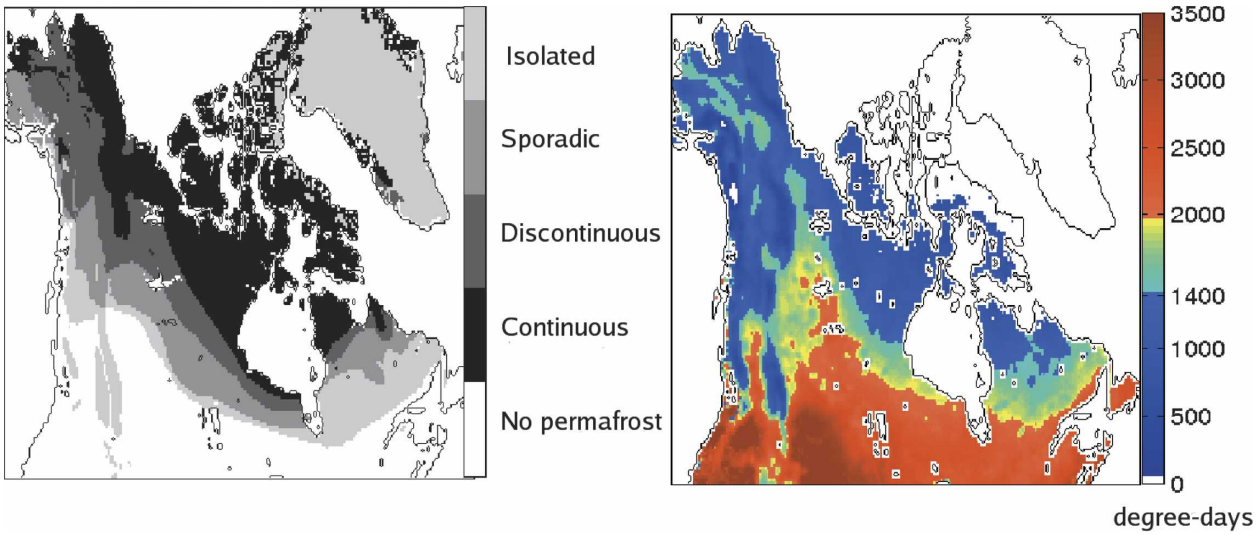

FIG. 9. (left) Heginbottom et al. (1993) permafrost zones distribution, and (right) mean (1992–2002) thawing index (degree-days) over Canada and Alaska.

6. Conclusions

This study is based on the method proposed by Fily et al. (2003) to derive the earth surface temperature time series from passive microwave observations (SSM/I EASE-Grid database). Their simple and robust method is used along with ERA-40 air temperatures to produce consistent hourly temperature series, with the aim of retrieving summer daily mean temperature interannual variations. A normalization scheme based on a diurnal model temperature is used to compensate for the data acquisition time variation as well as the problem of missing data resulting from the incomplete daily coverage below 50°N. This paper put the emphasis on the validation process by comparing results with in situ and gridded meteorological measurements, reanalysis datasets (ERA-40), and infrared satellite-derived skin temperature (ISCCP).

This work shows the potential of this approach and the use of passive microwaves for deriving a near-surface air temperature with an absolute accuracy on the order of 2.5°–3°C on a daily basis. However, the relative interannual variations are very close to those of ERA-40 and station data observed during the 1992–2002 period: Canada underwent an increase in temperature of $0.09° \pm 0.04°C\ yr^{-1}$, whereas a decrease of $-0.15° \pm 0.05°C\ yr^{-1}$ is observed over Alaska. Cumulative positive daily mean temperatures for snow-/ice-free pixels over the year are used to compute a thawing index, which can be related to permafrost distribution. The results show that the northern high latitudes registered a significant decrease (−7%) in the areas having a low thawing index. Changes in soil temperature associated with climate warming may result in thawing of permafrost, changes in terrain and hydrologic conditions, alteration of the distribution and growth rate of vegetation, enhancement of soil organic carbon decomposition, and increased gas emission (carbon dioxide and methane) from the soil to the atmosphere (Oechel et al. 1993; Trumbore et al. 1996; Anisimov and Nelson 1996; Nelson et al. 2001; Nelson 2003). These effects could have significant consequences locally (infrastructures, pipelines, etc.; ACIA 2004) and globally (hydrology; soil–atmosphere gas transfer).

Future works are thus needed to improve our knowledge of the annual magnitude, rates of change, and pattern of regional redistribution in surface temperature over northern latitudes under a changing climate. This implies a more accurate relationship definition between the satellite-derived surface temperature and the land cover. This technique will also be used along with a brightness temperature simulation model to derive a temperature of the top layer of snow during winter. Last, extending the time period with past data of SMMR and SSM/I (before 1992) sensors and recent series from SSM/I (still running) is also of major interest to address this key scientific question on the potential global warming impact.

Acknowledgments. Research funding was provided by the French Ministère de la Recherche (ACI Observation de la Terre, ACI Changement Climatique), the Ministère des Affaires Étrangères (Coopération France-Québec), the Canadian Fund for Climate and Atmospheric Sciences, the Canadian Natural Sciences and Engineering Research Council, Environment

Canada (CRYSYS project), and the Ouranos Consortium. We thank all of the providers of the datasets used: Marta Shulski (Alaska Climate Research Center) for air temperature from stations in Alaska, the BERMS Science and Management committees for providing the meteorological data for the Old Aspen site, Saskatchewan, Environment Canada for the meteorological data over Canada, the Canada Centre for Remote Sensing, Natural Resources Canada, for the land cover map, and the ECMWF for the reanalysis data.

REFERENCES

ACIA, 2004: *Impacts of a Warming Arctic: Arctic Climate Impact Assessment.* Cambridge University Press, 140 pp.

Aires, F., C. Prigent, W. Rossow, and M. Rothstein, 2001: A new neural network approach including first guess for retrieval of atmospheric water vapor, cloud liquid water path, surface temperature, and emissivities over land from satellite microwaves observations. *J. Geophys. Res.,* **106,** 14 887–14 907.

——, ——, and W. B. Rossow, 2004: Temporal interpolation of global surface skin temperature diurnal cycle over land under clear and cloudy conditions. *J. Geophys. Res.,* **109,** D04313, doi:10.1029/2003JD003527.

Anisimov, O., and P. Nelson, 1996: Permafrost distribution in the northern hemisphere under scenarios of climate change. *Global Planet. Change,* **14,** 59–72.

Armstrong, R., K. Knowles, M. Brodzik, and M. Hardman, 1994: DMSP SSM/I pathfinder daily EASE-Grid brightness temperatures. National Snow and Ice Data Center, digital media and CD-ROM (updated 2005).

Atkinson, D., and Coauthors, 2006: Canadian cryospheric response to an anomalous warm summer: A synthesis of the climate change action fund project "The State of the Arctic Cryosphere during the Extreme Warm Summer of 1998." *Atmos.–Ocean,* **44,** 347–375.

Basist, A., N. Grody, T. Peterson, and C. Williams, 1998: Using the Special Sensor Microwave/Imager to monitor land surface temperatures, wetness, and snow cover. *J. Appl. Meteor.,* **37,** 888–911.

Betts, R. A., J. H. Ball, A. Beljaars, M. Miller, and P. Viterbo, 1996: The land surface–atmosphere interaction: A review based on observational and global modeling perspectives. *J. Geophys. Res.,* **101,** 7209–7225.

Brown, R. D., 2000: Northern Hemisphere snow cover variability and change, 1915–97. *J. Climate,* **13,** 2339–2355.

——, and B. T. Alt, Eds., 2001: The state of the Arctic cryosphere during the extreme warm summer of 1998: Documenting cryospheric variability in the Canadian Arctic. Meteorological Service of Canada, Climate Research Branch, Downsview, ON, Canada, 33 pp. [Available online at http://www.socc.ca/summer/ftp/cispostersetc.html.]

Colton, M., and A. Poe, 1999: Intersensor calibration of DMSP SSM/I's: *F-8* to *F-14,* 1987–1997. *IEEE Trans. Geosci. Remote Sens.,* **37,** 418–439.

Dash, P., F. M. Göttsche, F. S. Olesen, and H. Fischer, 2002: Land surface temperature and emissivity estimation from passive sensor data: Theory and practice-current trends. *Int. J. Remote Sens.,* **23,** 2563–2594.

Davis, D., Z. Chen, H.-N. Nwang, L. Tsang, and E. Njoku, 1995: Solving inverse problems by Bayesian iterative inversion of a forward model with applications to parameter mapping using SMMR remote sensing data. *IEEE Trans. Geosci. Remote Sens.,* **33,** 1182–1193.

Fily, M., A. Royer, K. Goïta, and C. Prigent, 2003: A simple retrieval method for land surface temperature and fraction of water surface determination from satellite microwave brightness temperatures in sub-arctic areas. *Remote Sens. Environ.,* **85,** 328–338.

Hansen, J., A. Lacis, R. Ruedy, and M. Sato, 1992: Potential climate impact of Mount Pinatubo eruption. *Geophys. Res. Lett.,* **19,** 215–218.

——, R. Ruedy, M. Sato, and R. Reynolds, 1996: Global surface air temperature in 1995: Return to pre-Pinatubo level. *Geophys. Res. Lett.,* **23,** 1665–1668.

Heginbottom, J. A., J. Brown, E. S. Melnikov, and O. J. Ferrians, 1993: Circum-arctic map of permafrost and ground ice conditions. *Proceedings of the Sixth International Conference on Permafrost, Wushan, Guangzhou, China.* Vol. 2. South China University Press, 1132–1136. [Revised in 1997 by the National Snow and Ice Data Center/World Data Center for Glaciology.]

Jin, M., and R. E. Dickinson, 2002: New observation evidence for global warming from satellite. *Geophys. Res. Lett.,* **29,** 1400, doi:10.1029/2001GL013833.

Latifovic, R., Z.-L. Zhu, J. Cihlar, C. Giri, and I. Olthof, 2004: Land cover of North and Central America—Global Land Cover 2000. *Remote Sens. Environ.,* **89,** 116–127.

Lucht, W., and Coauthors, 2002: Climatic control on the high latitude vegetation greening trend and Pinatubo effect. *Science,* **296,** 1687–1689.

McFarland, M., R. Miller, and C. Neale, 1990: Land surface temperature derived from SSM/I passive microwave brightness temperature. *IEEE Trans. Geosci. Remote,* **28,** 839–844.

Mialon, A., 2005: Étude de la variabilité climatique des hautes latitudes nord, dérivée d'observations satellites micro-ondes (Study of northern high-latitude climatic variability, derived from microwave satellite observations). Ph.D., Université Joseph Fourier and Université de Sherbrooke, 230 pp. [Available online at http://www-lgge.ujf-grenoble.fr/publiscience/theses/theses.shtml.]

——, M. Fily, and A. Royer, 2005a: Seasonal snow cover extent from microwave remote sensing data: Comparison with existing ground and satellite based measurements. *EARSeL eProc.,* **4,** 215–225.

——, A. Royer, and M. Fily, 2005b: Wetlands seasonal dynamics and interannual variability over northern high latitudes, derived from microwave satellite data. *J. Geophys. Res.,* **110,** D17102, doi:10.1029/2004JD005697.

Nelson, F., 2003: (Un)frozen in time. *Science,* **299,** 1673–1675.

——, O. Anisimov, and N. Shiklomanov, 2001: Subsidence risk from thawing permafrost. *Nature,* **410,** 889–890.

Neumann, H. H., G. Den Hartog, R. Staebler, R. Mickle, and N. Trivett, 1995: Tower flux measurements at the BOREAS Old Aspen Tower Site. *Extended Abstracts, 29th Congress of the Canadian Meteorological and Oceanography Society,* Kelowna, BC, Canada, CMOS, 27–28.

New, M., M. Hulme, and R. Jones, 2000: Representing twentieth-century space–time climate variability. Part II: Development of a 1901–96 monthly terrestrial climate. *J. Climate,* **13,** 2217–2238.

Njoku, E. G., and L. Li, 1999: Retrieval of land surface parameters using passive microwaves measurements at 6–18 GHz. *IEEE Trans. Geosci. Remote Sens.,* **37,** 79–93.

Oechel, W. C., S. J. Hastings, G. Vourlitis, M. Jenkins, G. Riechers, and N. Grulke, 1993: Recent change of Arctic tundra ecosystems from a net carbon dioxide sink to a source. *Nature,* **361,** 520–523.

Oleke, C., T. Zhang, M. C. Serreze, and R. L. Amstrong, 2003: Regional-scale modeling of soil freeze/thaw over the Arctic drainage basin. *J. Geophys. Res.,* **108,** 4314, doi:10.1029/2002JD002722.

Overland, J. E., M. C. Spillane, D. B. Percival, M. Wang, and H. O. Mofjeld, 2004: Seasonal and regional variation of pan-Arctic surface air temperature over the instrumental record. *J. Climate,* **17,** 3263–3282.

Prigent, C., F. Aires, and W. B. Rossow, 2003: Land surface skin temperatures from a combined analysis of microwave and infrared satellite observations for an all-weather evaluation of the differences between air and skin temperatures. *J. Geophys. Res.,* **108,** 4310, doi:10.1029/2002JD002301.

Pulliainen, J. T., J. Grandell, and M. T. Hallikainen, 1997: Retrieval of surface temperature in boreal forest zone from SSM/I data. *IEEE Trans. Geosci. Remote Sens.,* **35,** 1188–1200.

——, ——, and J. Hallikainen, 1999: HUT snow emission model and its applicability to snow water equivalent retrieval. *IEEE Trans. Geosci. Remote Sens.,* **37,** 1378–1390.

Rossow, W. B., and R. A. Schiffer, 1991: ISCCP cloud data products. *Bull. Amer. Meteor. Soc.,* **72,** 2–20.

——, and L. C. Garder, 1993: Validation of ISCCP cloud detections. *J. Climate,* **6,** 2370–2393.

Smith, S., and M. M. Burgess, 1999: Mapping the sensitivity of Canadian permafrost to climate warming. *Interactions between the Cryosphere, Climate and Greenhouse Gases: Proceedings of the IUGG 99 Symposium HS2,* IAHS Publication 256, 71–80.

Traoré, P., A. Royer, and K. Goïta, 1998: Land surface temperature time series derived from weekly AVHRR GVI composite datasets: Potential and constraints for northern latitudes. *Canadian J. Remote Sens.,* **23,** 390–400.

Trumbore, S., O. Chadwick, and R. Amundson, 1996: Rapid exchange between soil carbon and atmospheric carbon dioxide driven by temperature change. *Science,* **272,** 393–395.

Uppala, S. M., and Coauthors, 2005: The ERA-40 re-analysis. *Quart. J. Roy. Meteor. Soc.,* **131,** 2961–3012.

Walker, A. E., J. L. Sokol, and M. R. Davey, 1997: Use of SSM/I 85 GHz passive microwave data for investigating Great Slave Lake ice freeze-up/break-up variations. *Proc. Int. Symp. on Geomatics in the ERA of RADARSAT* (GER'97), Ottawa, ON, Canada, CD-ROM.

Weng, R., and N. Grody, 1998: Physical retrieval of land surface temperature using the Special Sensor Microwave Imager. *J. Geophys. Res.,* **103,** 8839–8848.

Zhang, T., G. Barry, K. Knowles, A. Heginbottom, and J. Brown, 1999: Statistics and characteristics of permafrost and ground-ice distribution in the Northern Hemisphere. *Polar Geogr.,* **23,** 132–154.

Zhang, X., L. A. Vincent, W. D. Hogg, and A. Niitsoo, 2000: Temperature and precipitation trends in Canada during the 20th century. *Atmos.–Ocean,* **38,** 395–429.